

# Manifestations of Conformational Defects in Electronic Spectra of Polysilanes – a Theoretical Study

Barbora Hanulíková,<sup>\*1,2</sup> Ivo Kuritka<sup>1,2</sup>

**Summary:** In this paper, density functional theory (DFT) and time dependent DFT (TDDFT) are applied on the calculation of electronic properties of alkyl- and aryl-substituted oligosilanes with conformational defect introduced into their silicon chain. Oligo[methyl(phenyl)silane]s and oligo(dimethylsilane)s up to 10 or 13 mer units, respectively, are treated as model structures by DFT and TDDFT with B3LYP/6–31 G\* base. Frontier molecular orbital (FMO) energies evince the dependence on the presence as well as on the position of the defect in oligomer backbones. Delocalization of FMO is strongly influenced by position of the defect which in some cases divides the molecule to the FMO-rich part and the part almost without FMO delocalization and therefore affects location of electrons. Behaviour of longer chains in analogous polysilanes is deduced from linear regression of plots of FMO energy over the inverse of the polymerization degree.

**Keywords:** calculations; density functional theory; kink; polysilanes; UV-vis spectroscopy

## Introduction

Poly[(alkyl)silylene]s and poly[alkyl(aryl)silylene]s (generally called polysilylenes, organosilanes, polysilanes) evince noteworthy properties and therefore they have been of increased researchers interest for almost three decades. The uniqueness of these compounds lies predominantly in their electronic and thus optical properties that originate in electron delocalization along the chain which is made of silicon (Si) atoms connected by single bonds.<sup>[1,2]</sup> The delocalization or  $\sigma$ -conjugation is explained by overlapping of the lobes of  $sp^3$  hybridized silicone  $\sigma$ -orbitals of the particular or adjacent Si atoms (also called vicinal and germinal orbitals) as was reported else-

where.<sup>[3,4,5]</sup> Hence, absorption spectra of polysilanes have become indispensable knowledge and still investigated topic in the area of polymers and have been described, for instance, by<sup>[3,6,7]</sup> or UV-vis spectra of polysilanes-containing composites by.<sup>[8]</sup> The longest wavelength absorption around 300–350 nm is assigned to  $\sigma \rightarrow \sigma^*$  transition on Si-Si bond and it is known that the position of this absorption peak shifts with different side groups attached to the main chain. This was studied as early as in late 1980s by West, who measured absorption spectra of poly[methyl(phenyl)silane], poly[cyclo-hexyl(methyl)silane], poly[n-dodecyl(methyl)silane] and obtained wavelength maximum on 340 nm, 325 nm and 310 nm, respectively.<sup>[9]</sup> The description of excitation transitions of poly[methyl(phenyl)silane] was provided in detail in ref.<sup>[2]</sup> where combinations of transition  $\sigma \rightarrow \sigma^*$  on Si backbone and  $\pi \rightarrow \pi^*$  of phenyl are shown. Transition from silicon backbone to phenyl substituent through charge transfer, designed as  $\sigma \rightarrow \pi^*$ ,

<sup>1</sup> Polymer Centre, Faculty of Technology, Tomas Bata University in Zlín, namesti T. G. Masaryka 275, Zlín 76272, Czech Republic  
E-mail: hanulikova@ft.utb.cz

<sup>2</sup> Centre of Polymer Systems, University Institute, Tomas Bata University in Zlín, Nad Ovcírnou 3685, Zlín 76001, Czech Republic

was also found in ref.<sup>[10,11]</sup> Piqueras et al. have computed recently that the first and the second transition could be assigned as  $\sigma \rightarrow \pi^*$  and  $\sigma \rightarrow \sigma^*$ , respectively but the latter is probably located on Si-C bond instead the Si-Si bond.<sup>[12]</sup> Generally, UV-vis spectra of organosilanes are dependent on temperature, electric and magnetic field or used solvent.<sup>[5]</sup>

Another substantial fact is the effect of secondary polymer structure on the electron excitation and related properties. That is why polysilane conformations were also object of abundant research, both experimental and theoretical. The structural arrangement of polysilanes is described by particular dihedral angle, which consists of four consecutive silicon atoms and which can adopt six local energy minima designed as *cisoid* (C, 40°), *gauche* (G, 60°), *ortho* (O, 90°), *deviant* (D, 150°), *transoid* (T, 165°) and *anti* (A, 180°) conformation. There are two more states of arrangement, *syn* (S, 0°) and *eclipsed* (E, 120°), however, they are not stable conformations and cannot be caught and held for some time by polysilane structure.<sup>[13,14]</sup> All of the angle values can be either positive (+) or negative (–) and in proper cases (e.g. rod-like crystalline polysilanes with *deviant* or *transoid* conformation along the chain) can create right- or left-handed helix, respectively.<sup>[15,16]</sup> The planar conformation for silicone backbone is called *all-anti* (in the earlier papers *all-trans*), which means that each successive dihedral angle is about 180°. This is the case of rigid, crystalline and insoluble poly(dimethylsilane), as was shown in ref.<sup>[17]</sup> Fuzakawa et al. used cyclic oligosilane structure, which was attached to linear octasilane chain and prepared *all-anti* conformer that can offer maximum of  $\sigma$ -conjugation.<sup>[18]</sup>

Furthermore, some of the polysilanes are polymorphous. For example, poly(methyl-n-propylsilane) is able to adopt *deviant*, *transoid* and *all-anti* conformation in dependence on the temperature and processing history.<sup>[19]</sup> The optimum conformation is also influenced by polaron or exciton formation.<sup>[20]</sup> These quasiparticles

are also involved in the changes of electron density distribution as well as vibrational and absorption spectra.<sup>[21]</sup>

However, the regularity of the chain can be disrupted when one of its parts is forced to change its conformation. One of these defects can be demonstrated as a kink which creates a bend on the otherwise regular chain. Some theoretical research on this topic with oligosilanes as quantum wires has already been done in past.<sup>[22]</sup> Nevertheless, deeper investigation which can indicate the direct influence of the particular kink on electronic properties (energy of frontier orbitals, absorption maximum or delocalization of molecular orbitals) of polysilanes is still missing and therefore is the aim of this research paper.

As proved in many references above, nowadays, it is more and more usual to support or directly lead the investigations of structural, electronic or other properties of various molecules on the theoretical level. The foundations of these computations, which were based on the Schrödinger equation, were developed into the form of the density functional theory (DFT) and later time-dependent density functional theory (TDDFT) by Hohenberg, Kohn and Sham in the original papers from 1960.<sup>[23,24,25]</sup> In the present investigations, DFT is among the most popular quantum chemical theories which are able to work with the large number of models and basis sets, which give them the required flexibility for calculation of both the ground and excited molecular state.<sup>[26,27]</sup> Quantum chemistry provides a palette of theoretical approaches which are able to give trustworthy results. One of them is DFT/B3LYP method. It brings a little of ambiguity to a precise solution of some theoretical terms used in description of DFT in comparison with Hartree-Fock models, such as an exchange-correlation functional.<sup>[28]</sup> On the other hand, it corresponds well to experimental data of conjugated systems, as it has been successfully demonstrated in<sup>[12,29]</sup> to name a few. Time dependent extension of DFT provides

results which are close to experimental values for excitation energies of many chemical compounds<sup>[30,31]</sup> and in combination with hybrid model B3LYP, DFT provides good computation-experimental agreement with the statistical deviation of excitation energies about 0.5 eV.<sup>[28]</sup>

In the present paper, DFT and TDDFT are used to predict electron properties of poly[(dimethyl)silylene] (PDMSi) and poly[methyl(phenyl)silylene] (PMPSi) by extrapolation of results obtained for analogous oligomers with the backbone length from one to ten (in case of (dimethyl)silylene oligomers to thirteen) silicone atoms.

## Molecules and Computational Methods

Alkyl- and aryl-substituted oligosilanes were investigated using Spartan '08<sup>[32]</sup> computational software. Oligo[methyl(phenyl)silane]s (OMPSi<sub>n</sub>) and oligo[(dimethyl)silane]s (ODMSi<sub>n</sub>), where *n* is 1–10 and 1–13, respectively, were used as model molecules. The terminal silicone atoms in each oligosilane chain were capped with methyl groups.

Each molecule of OMPSi<sub>n</sub> and ODMSi<sub>n</sub> was optimized by DFT with B3LYP hybrid model and 6–31G\* polarization basis set. Structures of approximately *transoid* (OMPSi<sub>n</sub>) and *all-anti* (ODMSi<sub>n</sub>) conformation were attained in the first step of calculation. Afterwards, a set of semi empirical PM3 calculations was done to obtain energy profiles of the oligosilane conformers (*n* ≥ 4) with different values of the dihedral angle representing the kink. From the plot of energy against this dihedral angle, the most suitable conformers, i.e. those containing the kink were chosen and set as initial guess to another structural optimization by DFT/B3LYP 6–31G\* to obtain the new energy minimum and at the same time to have more precise geometry of the required kink. Ideally, four silicon atoms forming the kink would have *syn* conformation, however, it is not

the energetically favourable position for systems with bulky substituents, and thus the energy minimum is not possible to obtain with this geometry. Therefore, the set of calculations was carried out with a different but realistic initial value of the kink angle to find the minimum as close to the *syn* value as possible. After optimization, this angle was virtually measured with the result of 50–60° for all oligosilanes and thus the kink with an approximate conformation of *gauche* was formed. All of these calculations were made in the ground state of oligomers and at the same time no constraints of bonds and angles were set in the calculations. In addition, neither temperature nor solvent effect was considered, thus all molecules were virtually treated *in vacuo*.

To properly evaluate electronic properties, excited state calculations were run with TDDFT B3LYP model and 6–31G\* basis set. In this case, the single point energy was calculated with the initial geometry which was obtained in previous steps.

As a result, absorption wavelengths, excitation energies, intensities, molecular orbital energies and others were attained and they are commented in the following text.

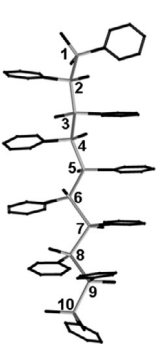
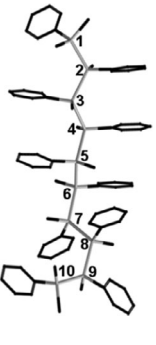
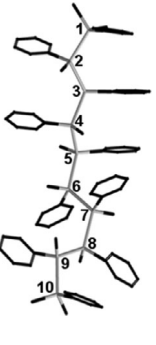
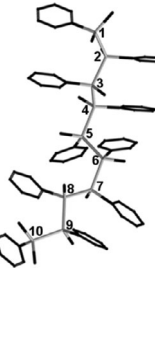
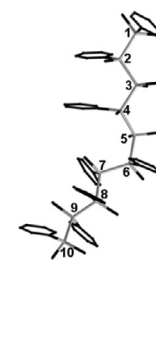

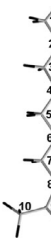



## Results and Discussion

### Geometry Optimization

*Gauche* conformation of the introduced kink was achieved during the optimization step in all studied molecules of OMPSi<sub>n</sub> and ODMSi<sub>n</sub>. Table 1 shows the optimized structures of decasilane oligomers and the position of the kink in the backbone to exemplify studied geometries. As can be seen, four kink positions can be obtained in decamer. The number of possible kink location is dependent on the length of the backbone, and from tetramer it increases by one per each two oligomers.

Oligosilane labels consist of a figure and a letter, where the first represents the number of silicon atoms in the backbone and the latter is the kink location. Carbon

**Table 1.**  
Optimized structures of decamer molecules with kink.

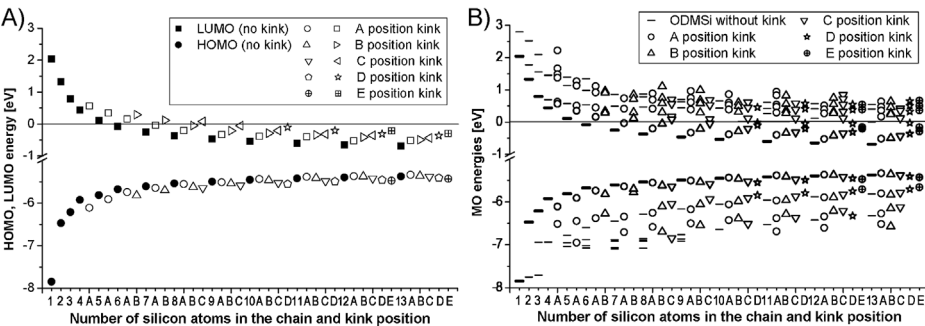
OMPSi				
10	10A	10B	10C	10D
				
ODMSi				
10	10A	10B	10C	10D
				

atoms are coloured in black and silicon atoms in light grey.

**Delocalization and Absorption Spectra**

The presence of the conformational defect represented by the kink causes significant

changes in molecular orbital (MO) energies in both alkyl- and aryl-substituted oligosilanes. Figure 1A depicts the highest and the lowest occupied molecular orbital (HOMO and LUMO, respectively) energies of ODMSi<sub>n</sub>. As can be clearly seen, LUMO



**Figure 1.**  
- HOMO, LUMO energies of ODMSi oligomers depicted in detail (A) and MO energy levels involved in excitation process (B).

energy levels are reduced from positive to negative values with the increasing number of repeated units. However, the situation is more complex for ODMSi<sub>n</sub> with the kink. In case of kinked ODMSi<sub>1–5</sub>, LUMO energies have positive values. Therefore LUMO energies can be assumed as stable up from the ODMSi<sub>6–9</sub>, where LUMOs reach negative values in dependence on the particular position of the kink. Furthermore, a presence of the kink itself causes increase in the LUMO energies and this trend continues substantially as the conformational defect position alters along the chain. In detail, the further from the end of the chain the kink is located, the higher the LUMO energy. The similar difference between LUMO of the chain with no kink and LUMO of the last possible oligomer with the kink can be seen in all ODMSi<sub>n</sub> and its value is around 0.4 eV. On the other hand, HOMO energy levels of ODMSi<sub>n</sub> evince opposite behaviour as their energy decreases with the kink position and generally they are affected to the lesser extent. Apparently, these energies stabilise when heptamer chain length is reached and further they stay on the similar level. In this case the scatter of values in HOMO energies between ODMSi<sub>n</sub> of the same chain length is around 0.1 eV.

Part B of Figure 1 shows all MO energy levels of ODMSi<sub>n</sub>, which are involved in the excitation process. As can be observed, energies of the levels above LUMO (supra-levels) are in most ODMSi<sub>n</sub> unstable, which corresponds with their UV-vis spectra. This fact can be seen in graphical inset in Table 2 which represents calculated UV-vis spectra of ODMSi<sub>10</sub>. The absorption maximum at 280–250 nm is assigned to HOMO→LUMO transition. As the kink changes its position further from the chain end, the maximum absorption wavelength ( $\lambda_{\max}$ ) is shifted to lower values and therefore the band gap increases. Another fact is that with increasing values of LUMO energies in dependence on the kink position, the LUMO + 1 level evince complementary decrease approaching the frontier energy level.

Figures 2A, 2B and graphical inset in Table 3 show MO energies and UV-vis spectra of OMPSi<sub>n</sub>. When compared with ODMSi<sub>n</sub>, the main difference lies in the fact that all LUMO energies have stable negative values and HOMO energies are slightly more influenced than LUMO energy level by the kink presence and position.

Although the variations in energy values (LUMO around 0.1 eV, HOMO 0.15 eV) are not so evident as in ODMSi<sub>n</sub>, the clear shift is observable in absorption spectra in Table 3. The band gap is created between HOMO and supra-LUMO levels in OMPSi<sub>n</sub> (detailed assignments are also provided in Table 3) and combines  $\sigma \rightarrow \sigma^*$  transitions and  $\sigma \rightarrow \pi^*$ . HOMO→LUMO transition is realised in cases with LUMO delocalized along the backbone not only along aromatic substituents, as can be seen in Figure 4.

Computed values of both ODMSi<sub>n</sub> and OMPSi<sub>n</sub> excitation energies (E) are slightly overestimated (around 0.5 eV) in comparison with experimental results published in.<sup>[2,33,34]</sup>

Delocalization of MO along the molecules of ODMSi<sub>n</sub> and OMPSi<sub>n</sub> is of essential importance. Figure 3 and Figure 4 display delocalization of HOMO, LUMO and other MO involved in UV-vis absorptions of ODMSi<sub>n</sub> and OMPSi<sub>n</sub>, respectively. The most important are HOMOs and LUMOs as they determine the absorption edge and maximum.

ODMSi<sub>10</sub> without the kink has both FMO (Frontier Molecular Orbitals) delocalized equally along the whole chain length. On the contrary, 10A, 10B and 10C oligomers seem to be divided into two parts by the introduced kink. Equal delocalization is kept only on the longer part of the chain and reaches the centre of the defect. At the same time, the rest of the molecule, representing the shorter part of the molecule, is almost completely without FMOs delocalization. This influence of *gauche* conformation occurs when the kink divides the structure into asymmetric parts. Therefore, in the case of 10D this effect disappears and FMOs are delocalized along the whole chain as in 10 because of perfect symmetry.

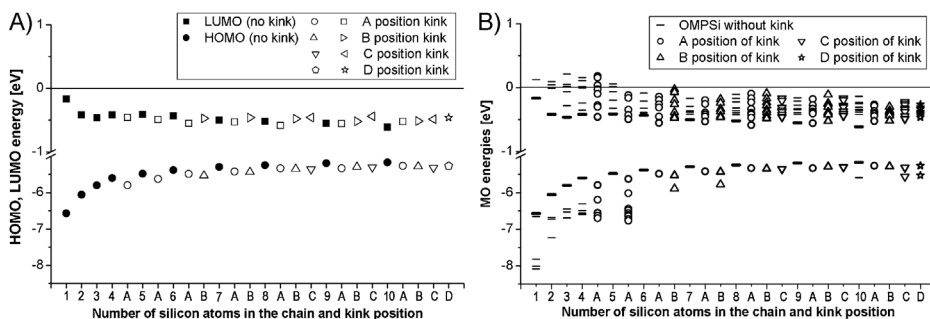
**Table 2.**Calculated UV-vis spectra and excitation process data of ODMSi<sub>10</sub>.

UV-vis spectra of ODMSi <sub>10</sub>						ODMSi 10					
Intensity [a.u.]						E [eV]	λ [nm]	M	I [a.u.]	MO	A
						4.3732	284	S	2.0023	H→L	0.985
						5.1307	242	S	0	H-1→L	0.983
						5.1522	241	S	0.0002	H→L + 2	0.967
						5.3956	230	S	0	H-1→L + 2 H→L + 3	-0.357 0.908
						5.4448	228	S	0	H→L + 1	0.980
Wavelength [nm]						5.685	218	S	0.0021	H-2→L	0.977

ODMSi 10A						ODMSi 10B					
E [eV]	λ [nm]	M	I [a.u.]	MO	A	E [eV]	λ [nm]	M	I [a.u.]	MO	A
4.4985	276	S	1.6962	H→L	0.985	4.6187	268	S	1.5149	H→L	0.982
5.0854	244	S	0.0004	H→L + 1	0.946	5.0934	243	S	0.0105	H→L + 1	0.881
										H→L + 2	0.373
5.2453	236	S	0.0060	H-1→L	0.970	5.2139	238	S	0.0501	H-1→L	0.951
5.2960	234	S	0.0011	H-1→L + 1	0.296	5.2984	234	S	0.0878	H→L + 1	-0.332
				H→L + 2	0.759					H→L + 2	0.676
				H→L + 3	0.487					H→L + 3	0.549
5.5063	225	S	0.0048	H-2→L	0.403	5.4693	227	S	0.0673	H→L + 2	-0.580
				H→L + 2	-0.457					H→L + 3	0.712
				H→L + 3	0.690						
				H→L + 4	0.294						
5.5675	223	S	0.0013	H-2→L	0.828	5.6203	221	S	0.0279	H-2→L	0.957
				H→L + 2	0.295						
				H→L + 3	-0.371						

ODMSi 10C						ODMSi 10D					
E [eV]	λ [nm]	M	I [a.u.]	MO	A	E [eV]	λ [nm]	M	I [a.u.]	MO	A
4.7671	260	S	1.3360	H→L	0.965	4.9064	253	S	1.4185	H-1→L	-0.253
										H→L + 1	0.946
5.0506	245	S	0.1738	H→L + 1	0.908	4.9758	249	S	0.1583	H-1→L	0.977
				H→L + 2	-0.305						
5.1904	239	S	0.2784	H-1→L	0.923	5.1751	240	S	0.4305	H-1→L	0.874
				H→L + 2	0.238					H→L + 2	0.398
5.2850	235	S	0.1265	H→L + 1	0.294	5.3250	233	S	0.0259	H-1→L	-0.368
				H→L + 2	0.807					H-1→L + 3	-0.294
				H→L + 3	-0.364					H→L + 1	-0.223
										H→L + 2	0.841
5.4329	228	S	0.0156	H-1→L + 1	-0.495	5.3279	233	S	0.0977	H-1→L + 1	0.796
				H-1→L + 2	0.315					H-1→L + 2	0.342
				H→L + 2	0.321					H→L + 3	-0.454
				H→L + 3	0.633						
5.5279	224	S	0.2325	H-1→L + 1	0.788	5.4586	227	S	0.0575	H-1→L + 1	0.570
				H→L + 3	0.480					H-1→L + 2	-0.383
										H→L + 3	0.688

E [eV] – excitation energy; λ [nm]– wavelength; M – multiplicity; I [a.u.] – intensity (oscillator strength); MO – molecular orbital; A –amplitude; S – singlet

**Figure 2.**

HOMO, LUMO energies of OMPSi oligomers depicted in detail (A) and MO energy levels involved in excitation process (B).

**Table 3.**

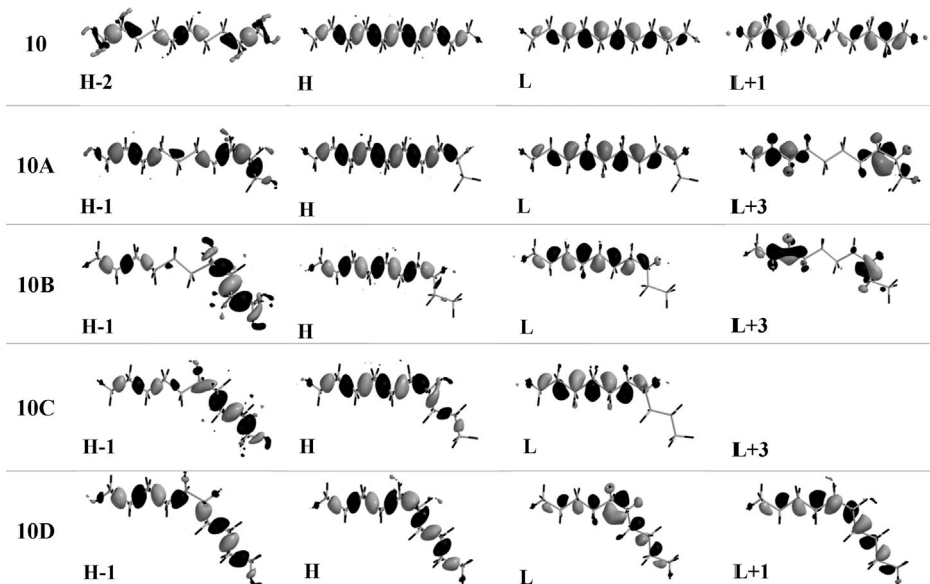
UV-vis spectra and excitation process data of OMPSi<sub>10</sub>. For explanation of symbols and abbreviations see the legend in Table 2.

UV-vis spectra of OMPSi <sub>10</sub>						OMPSi 10					
	10D					E [eV]	λ [nm]	M	I [a.u.]	MO	A
						4.0063	309	S	1.3942	H→L	0.971
						4.2826	290	S	0.0676	H→L+1	0.937
						4.3214	287	S	0.0438	H→L+2	0.845
										H→L+3	-0.270
										H→L+5	-0.235
										H→L+6	0.246
						4.3360	286	S	0.0354	H→L+2	0.334
										H→L+3	0.847
										H→L+6	-0.302
10C										H→L+3	-0.279
										H→L+4	0.577
										H→L+5	-0.348
										H→L+6	-0.467
										H→L+7	0.410
10B										H-1→L	0.245
										H→L+4	0.598
										H→L+6	0.221
										H→L+7	-0.600
10A											
10											

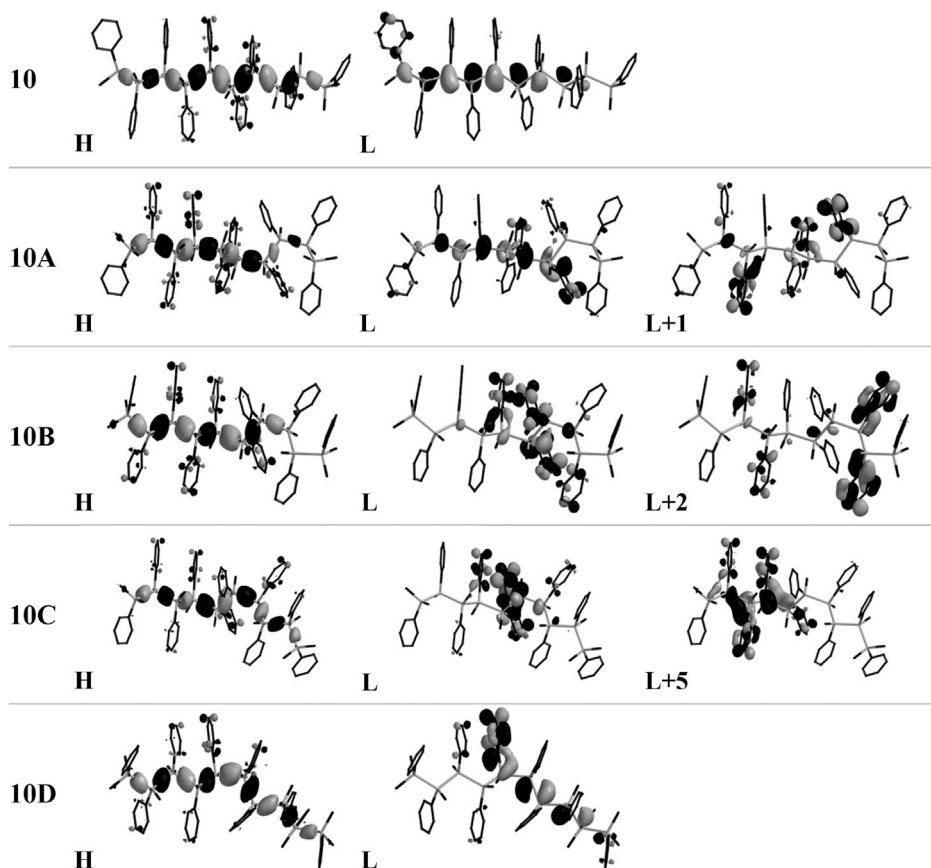
(Continued)

Table 3. (Continued)

OMPSi 10A						OMPSi 10B					
4.4663	278	S	0.0230	H→L + 2 H→L + 6	−0.239 −0.908	4.4628	278	S	0.1222	H→L + 1 H→L + 2 H→L + 3 H→L + 5	0.532 0.420 −0.517 −0.365
4.502	275	S	0.0690	H→L + 2 H→L + 3 H→L + 4	0.299 0.789 −0.285	4.4916	276	S	0.0354	H→L + 2 H→L + 4 H→L + 5	0.424 −0.332 0.724
OMPSi 10C						OMPSi 10D					
E [eV]	λ [nm]	M	I [a.u.]	MO	A	E [eV]	λ [nm]	M	I [a.u.]	MO	A
4.3319	286	S	0.4887	H→L	0.969	4.2649	291	S	0.8493	H→L	0.940
4.3769	283	S	0.1233	H→L + 1 H→L + 2 H→L + 5	0.856 −0.303 −0.235	4.3408	286	S	0.2485	H→L + 1 H→L + 2 H→L + 3 H→L + 4 H→L + 1 H→L + 2 H→L + 3	−0.527 0.496 0.529 0.334 0.801 0.407 0.344
4.4485	279	S	0.2987	H→L + 1 H→L + 1 H→L + 2 H→L + 5	0.257 0.388 0.772 0.290	4.3715	284	S	0.1900	H→L + 1 H→L + 2 H→L + 3	−0.561 0.676 −0.267
4.4859	276	S	0.2510	H→L + 5 H→L + 2 H→L + 5 H→L + 6	−0.222 −0.388 0.776 −0.224	4.4296	280	S	0.0124	H→L + 3 H→L + 4 H→L + 6	−0.561 0.676 −0.267
4.5331	274	S	0.1059	H→L + 2 H→L + 3 H→L + 4 H→L + 6	−0.281 0.594 0.471 −0.451	4.4571	278	S	0.0736	H→L + 2 H→L + 2 H→L + 3 H→L + 4 H→L + 5 H→L + 6	0.298 0.575 0.321 −0.339 0.331 −0.416
4.5449	273	S	0.0424	H→L + 2 H→L + 3 H→L + 3 H→L + 4 H→L + 7	−0.250 −0.224 −0.478 0.591 −0.399	4.5029	275	S	0.0463	H→L + 4 H→L + 2 H→L + 4 H→L + 5 H→L + 6	0.240 −0.311 0.318 0.737 0.256







**Figure 4.**

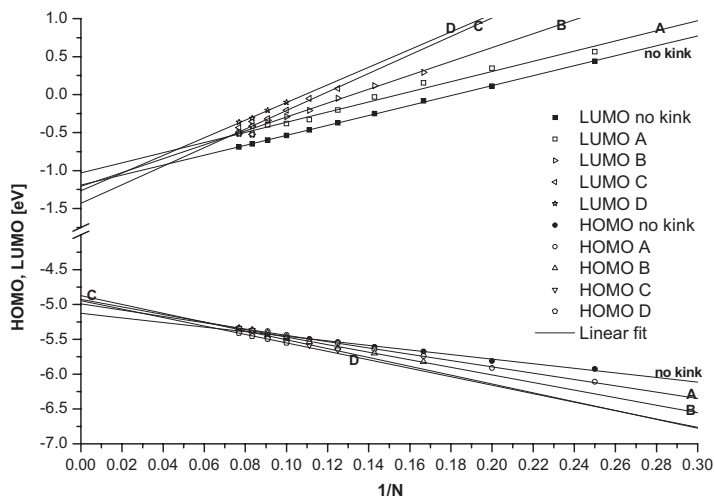
Molecular orbitals of OMPSi<sub>10</sub>—positive MO grey, negative MO black.

In OMPSi<sub>10</sub> the situation is partially different. Previous claims on orbital delocalization and density distribution are valid only for HOMOs. LUMOs are also delocalized to phenyl rings to some extent and in some cases (10B and 10C) they are located mostly on the rings which are attached exactly to the defect part of the structure. This indicates possible trap sites for eventual charge transfer state generation. In next, the symmetry of LUMOs involving  $\sigma$ - $\pi$  mixing with  $\pi$  orbitals of phenyl groups helically arranged along the chain is not that perfect as in purely  $\sigma$ -like LUMOs of ODSi<sub>n</sub> in case of the D-position of the kink. It can be seen in Figure 4 that a delocalisation of the OMPSi<sub>10</sub> LUMO spreads from the chain over a phenyl group in suitable position extending thus the

conjugation length in one direction which is probably more energetically favourable than delocalisation over the other part of the chain which would be shorter.

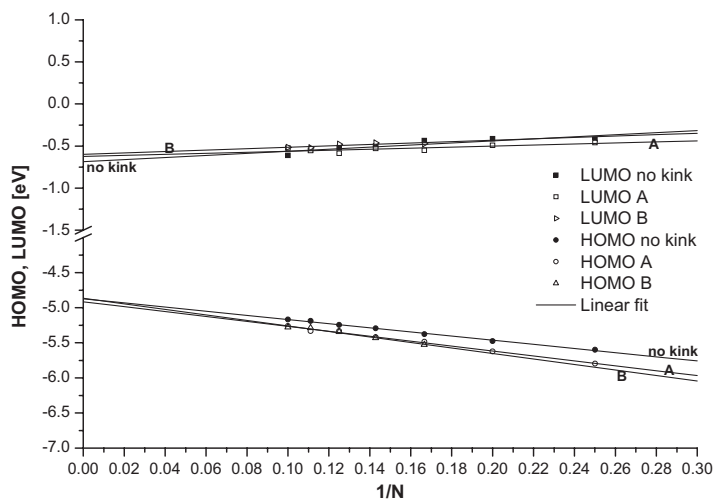
#### Extrapolation to Polysilanes

The number of oligomers which served as model molecules was chosen according to the computational time convenience. OMP-Si<sub>n</sub> were therefore investigated to decamers, while ODSi<sub>n</sub> to tridecamers. Obtained HOMO and LUMO energies were then plotted as a function of reciprocal number of Si atoms in the chain ( $1/N$ ) with linear regression. For the purpose of linearization, the first three values (monomer to trimer) of FMO energies were omitted as they cannot represent the defect structure involving four Si atoms at all. The



**Figure 5.**

Linear regression of ODMSi<sub>n</sub> LUMO and HOMO energies vs. 1/N, N > 3.



**Figure 6.**

- Linear regression of OMPSi<sub>n</sub> LUMO and HOMO energies vs. 1/N, N > 3.

properties of higher polymeric chains can therefore be predicted. Figure 5 and Figure 6 illustrate linearized dependence of MO energies on the chain length for ODMSi<sub>n</sub> with the kink at A, B, C and D position and OMPSi<sub>n</sub> with the kink at A and B position, respectively. As can be seen, this fitting curve was chosen in vast majority of cases properly as the points are in agreement with linear function (predicted values

of FMO energies for polymer-size backbones, mean errors and coefficients of determination are listed in Table 4). The exception in these reliable linear trends is the dependence of LUMO energies of PMPSi on 1/N where coefficients of determination are only around 0.6.

FMO energy values for infinite defectless chain were predicted ( $-0.69 \pm 0.05$ ) eV and ( $-4.87 \pm 0.01$ ) eV for PMPSi and

**Table 4.**

Linear regression data

PDMSi	HOMO (poly)	R <sup>2</sup>	LUMO (poly)	R <sup>2</sup>
no kink	$-5.13 \pm 0.01$	0.995	$-1.19 \pm 0.01$	1.000
A	$-4.99 \pm 0.01$	0.998	$-1.03 \pm 0.04$	0.985
B	$-4.94 \pm 0.02$	0.996	$-1.16 \pm 0.03$	0.996
C	$-4.97 \pm 0.03$	0.989	$-1.28 \pm 0.05$	0.991
D	$-4.95 \pm 0.02$	0.997	$-1.27 \pm 0.06$	0.993
PMPSi	HOMO (poly)	R <sup>2</sup>	LUMO (poly)	R <sup>2</sup>
no kink	$-4.87 \pm 0.01$	0.995	$-0.69 \pm 0.05$	0.788
A	$-4.91 \pm 0.02$	0.993	$-0.62 \pm 0.04$	0.613
B	$-4.87 \pm 0.04$	0.989	$-0.60 \pm 0.05$	0.676

( $-1.19 \pm 0.01$ ) eV and ( $-5.13 \pm 0.01$ ) eV for PDMSi. Introduction of the kink at the end of a semi-infinite chain causes observable decrease of LUMO energy from  $-0.69$  eV to  $-0.6$  eV for PMPSi and has no effect on its HOMO energy level. The opposite effect can be observed for PDMSi. In this case, the kink at the end of a semi-infinite chain slightly elevates HOMO level from  $-5.13$  eV to  $-4.9$  eV and there is almost no effect on LUMO energy. When deviations of HOMO and LUMO energies for infinite chain length are considered, it can be said that the fitting curves meet in one point, which is expectable due to the presumption that the kink, which is located in the backbone as was described above, does not significantly influence properties of very long molecules without any other defect. In addition, overall precision cannot be better than  $0.5$  eV which arises from the application of DFT.

Beside extrapolation, we claim that the other findings obtained for treated oligomers hold on for long chain polymers adequately as well.

## Conclusion

Delocalization of molecular orbitals is very asymmetric and localized to the longer segment when conformational defect, here presented by the kink of *gauche* conformation, is introduced into silicon backbones of both alkyl- and aryl-substituted oligosilanes. This causes the shift of absorption maxima to lower wavelengths as the

position of the kink is moved to the centre of the chain, in other words, the conjugated segments become shorter. If the linearity of polysilane chain is disrupted FMOs are located on longer segments as they allow greater extent of delocalization. A fully symmetric situation can occur for oligomers with even number of Si atoms which mean that no segment is energetically favourable as they are of the same length. For LUMO in OMPSi oligomers, this can be corrupted locally with the contribution of phenyl group which is in suitable position with respect to one of the two segments.

FMO energy also evinces clear dependence on the kink location. Generally, in both studied types of structures, HOMO energies decrease while LUMO energies increase as the *gauche* defect alters its position to the centre of the backbone. In case of PMPSi the kink is expected to be the potential trap site for charge transfer complex formation. However, optimal geometries of molecules in excited states have not been addressed in this study because the computational time is too high.

**Acknowledgement:** This work was supported by the Internal Grant Agency of Tomas Bata University in Zlin (grant No. IGA/FT/2013/025). This paper was written with support of Operational Program Research and Development for Innovations co-funded by the European Regional Development Fund (ERDF) and national budget of the Czech Republic, within the framework of project Centre of Polymer Systems (reg. number: CZ.1.05/2.1.00/03.0111) and with support of Operational Program Education for Competitiveness co-funded by

the European Social Fund (ESF) and national budget of the Czech Republic, within the framework of project Advanced Theoretical and Experimental Studies of Polymer Systems (reg. number: CZ.1.07/2.3.00/20.0104).

- [1] Y. V. Demchenko, J. Klimovic, S. Nespurek, *Macromol. Symp.* **2004**, 212, 461.
- [2] C. C. Phifer, W. J. Thomes, K. Simmnos-Potter, B. G. Potter, *J. Chem. Phys.* **2004**, 120, 1613.
- [3] S. Nespurek, G. Wang, K. Yoshino, *J. Optoelectron. Adv. M.* **2005**, 7, 223.
- [4] V. V. Semenov, *Russ. Chem. Rev.* **2011**, 80, 313.
- [5] J. E. Mark, H. R. Allcock, R. West, "Inorganic Polymers", Oxford University Press, New York **2005**, p. 200.
- [6] A. Watanabe, *J. Organomet. Chem.* **2003**, 685, 122.
- [7] H. Lei, C. Baoxue, I. Mamoru, *Opt. Mater.* **2011**, 33, 452.
- [8] R. Shankar, U. Sahoo, V. Shahi, *Macromolecules* **2011**, 44, 3240.
- [9] R. West, *J. Organomet. Chem.* **1986**, 300, 327.
- [10] S. Nespurek, J. Sworakowski, A. Kadashchuk, P. Toman, *J. Organomet. Chem.* **2003**, 685, 269.
- [11] S. Nespurek, A. Eckhardt, *Polym. Adv. Technol.* **2001**, 12, 427.
- [12] M. C. Piqueras, R. Crespo, J. Michl, *J. Phys. Chem. A* **2008**, 112, 13095.
- [13] J. Michl, R. West, *Accounts Chem. Res.* **2000**, 33, 821.
- [14] H. A. Fogarty, C.-H. Ottosson, J. Michl, *J. Mol. Struc. Teochem.* **2000**, 506, 243.
- [15] M. Fujiki, *J. Organomet. Chem.* **2003**, 685, 15.
- [16] T. Karatsu, *J. Photoch. Photobio. C* **2008**, 9, 111.
- [17] S. Furukawa, H. Ohta, *Thin Solid Films* **2003**, 438, 48.
- [18] A. Fuzakawa, H. Tsuji, K. Tamao, *J. Am. Chem. Soc.* **2006**, 128, 6800.
- [19] S. V. Bukalov, Y. V. Zubavichus, L. A. Leites, J. R. Koe, R. West, *Polymer* **2009**, 50, 4845.
- [20] P. Toman, *Synthetic Met.* **2000**, 109, 259.
- [21] J. Nozar, S. Nespurek, J. Sebera, *J. Mol. Model.* **2012**, 18, 623.
- [22] H. Taremae, N. Matsumoto, *Solid State Commun.* **1996**, 99, 917.
- [23] P. Hohenberg, W. Kohn, *Phys. Rev.* **1964**, 136, B864.
- [24] W. Kohn, L. J. Sham, *Phys. Rev.* **1965**, 140, A1133.
- [25] M. A. L. Marques, E. K. U. Gross, *Annu. Rev. Phys. Chem.* **2004**, 55, 427.
- [26] M. E. Casida, *J. Mol. Struc. Teochem.* **2009**, 914, 3.
- [27] K. Burke, J. Werschnik, E. K. U. Gross, *J. Chem. Phys.* **2005**, 123, 062206.
- [28] R. Bauernschmitt, R. Ahlrichs, *Chem. Phys. Lett.* **1996**, 256, 454.
- [29] R. Crespo, M. C. Piqueras, J. Michl, *Theor. Chem. Acc.* **2007**, 118, 81.
- [30] M. Promkatkaew, S. Suramitr, T. Karpkird, M. Ehara, S. Hannongbua, *Int. J. Quantum Chem.* **2013**, 113, 542.
- [31] A. Dreuw, M. Head-Gordon, *Chem. Rev.* **2005**, 105, 4009.
- [32] CA. Y. Spartan, '08 Wavefunction Inc, Irvine. L. F. Shao, Y. Molnar, J. Jung, S. T. Kussmann, C. Brown, A. T. B. Ochsenfeld, L. V. Gilbert, S. V. Slipchenko, D. P. Levchenko, R. A. O'Neill, R. C. DiStasio, Jr., T. Lochan, G. J. O. Wang, N. A. Beran, J. M. Besley, C. Y. Herbert, T. Lin, S. H. Van Voorhis, A. Chien, R. P. Sodt, V. A. Steele, P. E. Rassolov, P. P. Maslen, R. D. Korambath, B. Adamson, J. Austin, E. F. C. Baker, H. Byrd, R. J. Dachsels, A. Doerksen, B. D. Dreuw, A. D. Dunietz, T. R. Dutoi, S. R. Furlani, A. Gwaltney, S. Heyden, C.-P. Hirata, G. Hsu, R. Z. Kedziora, P. Khalliulin, A. M. Klunzinger, M. S. Lee, W. Z. Lee, I. Liang, N. Lotan, B. Nair, E. I. Peters, P. A. Proynov, Y. M. Pieniazek, J. Rhee, E. Ritchie, C. D. Rosta, A. C. Sherrill, J. E. Simmonett, H. L. Subotnik, I. I. Woodcock, W. Zhang, A. T. Bell, A. K. Chakraborty, D. M. Chipman, F. J. Keil, A. Warshel, W. J. Hehre, H. F. Schaefer, J. Kong, A. I. Krylov, P. M. W. Gill, M. Head-Gordon, *Phys. Chem. Chem. Phys.* **2006**, 8, 3172.
- [33] N. Matsomoto, *Jpn. J. Appl. Phys.* **1998**, 37, 5425.
- [34] Y. A. Skryshevskii, *J. Appl. Spectrosc.* **2003**, 70, 855.